Conventional and High-Speed Intravital Multiphoton Laser Scanning Microscopy of Microvasculature, Lymphatics, and Leukocyte–Endothelial Interactions

Timothy P. Padera,[1,2,3] Brian R. Stoll,[1,3]* Peter T.C. So,[3] and Rakesh K. Jain[1,2,3]*

[1]Massachusetts General Hospital, Boston, MA; [2]Harvard Medical School, Cambridge, MA; [3]Massachusetts Institute of Technology, Cambridge, MA

Abstract

The ability to determine various functions of genes in an intact host will be an important advance in the postgenomic era. Intravital imaging of gene regulation and the physiological effect of the gene products can play a powerful role in this pursuit. Intravital epifluorescence microscopy has provided powerful insight into gene expression, tissue pH, tissue pO_2, angiogenesis, blood vessel permeability, leukocyte–endothelial (L–E) interaction, molecular diffusion, convection and binding, and barriers to the delivery of molecular and cellular medicine. Multiphoton laser scanning microscopy (MPLSM) has recently been applied in vivo to overcome three drawbacks associated with traditional epifluorescence microscopy: (i) limited depth of imaging due to scattering of excitation and emission light; (ii) projection of three-dimensional structures onto a two-dimensional plane; and (iii) phototoxicity. Here, we use MPLSM for the first time to obtain high-resolution images of deep tissue lymphatic vessels and show an increased accuracy in quantifying lymphatic size. We also demonstrate the use of MPLSM to perform accurate calculations of the volume density of angiogenic vessels and discuss how this technique may be used to assess the potential of antiangiogenic treatments. Finally, high-speed MPLSM, applied for the first time in vivo, is used to compare L–E interactions in normal tissue and a rhabdomyosarcoma tumor. Our work demonstrates the potential of MPLSM to noninvasively monitor physiology and pathophysiology both at the tissue and cellular level. Future applications will include the use of MPLSM in combination with fluorescent reporters to give novel insight into the regulation and function of genes. *Mol Imaging* (2002) **1,** 9–15.

Keywords: Fluorescence microscopy, multiphoton laser scanning microscopy, tumor pathophysiology, angiogenesis, lymphatics, leukocyte–endothelial interaction.

Introduction

Over the past 75 years, many chronic animal models have been developed to investigate physiology and pathophysiology using intravital microscopy [1]. These models overcome limitations associated with more traditional histological techniques. More specifically, they allow for the study of biological events without loss of temporal dynamics or in vivo microenvironment. Intravital epifluorescence microscopy has been used in combination with these models to measure gene expression [2], permeability of blood vessels [3], cell interactions [4,5], and cell transport [6,7], as well as diffusion [8], convection [9] and binding [10], pO_2, and pH [11]. The information gained from these measurements is crucial to understanding molecular and cellular processes underlying physiology and pathophysiology and to the design and delivery of molecular therapy.

In the postgenomic era, many challenges remain and intravital microscopy is well tailored to address two of these in particular. First, the function and regulation of many newly described genes remains unknown [12]. Novel approaches to determining the regulation and function of these genes in vivo will be critical to understanding their role [2]. Second, the ability to alter gene expression and potentially repair mutated genes will require effective delivery of macromolecules to the target tissue [13]. This will require studying the transport of these macromolecules in blood, the lymphatic system, and the interstitial compartment of the tissue to understand and overcome the barriers that impede their delivery and efficacy. These two challenges are particularly pertinent in a solid tumor, a genetically unstable target that presents substantial obstacles to the delivery and effectiveness of macromolecular therapy, for example, gene therapy. However, three-dimensional resolution and deeper imaging depth are needed to enable high-resolution intravital imaging to reach its full potential. Confocal microscopy, used extensively in bioimaging applications, permits acquisition of three-dimensional information by eliminating out-of-focus light through the use of a pinhole. However, the energy delivered by the excitation light causes extensive photodamage to living tissues [14], and the use of a pinhole, along with descanning and short wavelength light, limits the depth of signal detection to $\sim$100 μm.

Abbreviations: MPLSM, multiphoton laser scanning microscopy; L–E, leukocyte–endothelial; GFP, green fluorescent protein; PMT, photomultiplier tube.

Corresponding author: Rakesh K. Jain, Department of Radiation Oncology, Massachusetts General Hospital, Boston, MA 02114.

Received 12 July 2001; Accepted 3 August 2001.

*Those authors contributed equally to this work.

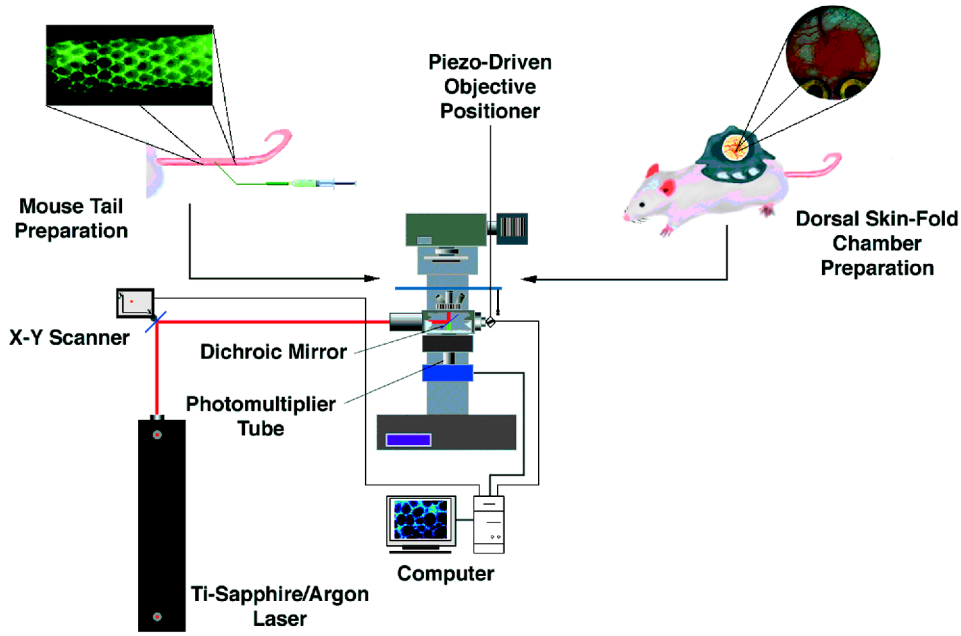

Figure 1. *Schematic diagram of the multiphoton laser scanning microscopy apparatus used for experiments. Mice bearing dorsal skin-fold preparations were restrained on the stage of the inverted microscope and normal and tumor microvasculature was visualized through a window in the chamber. The same setup was used in the mouse tail microlymphangiography experiments. For high-speed MPLSM, one of the galvanometer-driven mirrors in the X–Y scanner was replaced by a rotating polygonal mirror to produce faster scans in the x direction. Additionally, the single-photon counting PMT was replaced by a high-sensitivity PMT in order to handle the high-signal photon flux in video-rate imaging.*

Recently, multiphoton laser scanning microscopy (MPLSM) [15] has been applied to in vivo systems [14,16–21]. MPLSM represents a significant improvement over traditional epi-fluorescence microscopy, which has the following limitations in vivo: (i) scattering of excitation and emission light limits imaging depth, leaving tissue structure and function below approximately 10–40 μm concealed; and (ii) out-of-focus light from three-dimensional structures is projected onto a two-dimensional plane, yielding surface-weighted images and measurements. MPLSM overcomes these limitations by using longer-wavelength light, which penetrates deeper into tissue. The excitation of a fluorophore using infrared light requires the simultaneous absorption of two photons [22]. Consequently, excitation in MPLSM occurs only at the focal point of the objective, giving high x–y–z spatial resolution while eliminating the need for a pinhole to block out-of-focus light, resulting in less tissue phototoxicity.

One disadvantage of conventional MPLSM is the slow imaging speed (~1–2 frames/sec for high resolution). This is particularly problematic when studying blood flow and L–E interactions. Although a technique has been developed to measure steady blood velocity [19,21], imaging of more complicated short time scale phenomena in vivo has, until now, not been demonstrated. The speed at which an image can be acquired is dependent on the ability of two galvanometer-driven mirrors to move the laser across the x–y plane of the image. Recently, a high-speed multiphoton laser scanning microscope has been developed [23] that replaces one of the slow galvanometer driven mirrors with a high-speed, rotating polygonal mirror allowing acquisition of up to 100 frames/sec.

The current work builds upon and extends our recently published study [21]. We applied conventional, as well as high-speed, MPLSM to study the pathophysiology of solid tumors (Figure 1). First, we imaged lymphatics for the first time, which play a role in the spread of cancer to distant sites, as well as in the development of elevated interstitial fluid pressure inside tumors. Second, we imaged angiogenic blood vessels, which supply a growing tumor with oxygen, provide a pathway for the hematogenous dissemination of cancer to distant sites, and serve as a conduit for the delivery of systemic therapies. These vessels are also the target of potential antiangiogenic treatments. Finally, we used high-speed MPLSM to image the interaction of leukocytes with the endothelium (L–E interactions). L–E interactions are important in monitoring the ability of the immune system to control tumor spread and also serve as a marker of stimulated endothelium.

Materials and Methods

Intravital MPLSM

The construction of the multiphoton laser scanning microscope (Figure 1) has been described previously [24]. Briefly, a femtosecond mode-locked Ti-sapphire laser (Mira 900; Coherent, Palo Alto, CA) tuned to a wavelength of 780 nm was directed into the microscope by a galvanometer-driven x–y scanner (Cambridge Technology, Watertown, MA). A Glan-Thomson polarizer adjusted the power of the incident laser. The laser light entered a Zeiss Axiovert 110 microscope (Zeiss,

Thornwood, NY) where it deflected into the objective by a custom-made dichroic mirror (Chroma Technology, Brattleboro, VT). A Zeiss Achroplan 20×/0.5 NA/water objective and a Zeiss Achroplan 10×/0.3 NA/water objective were used. The axial position was set by a piezo-driven objective positioner, which was controlled by the data acquisition computer. The fluorescence emission was collected by the same objective, passed through the dichroic mirror and barrier filter (short pass 2 mm BG-39 Schott glass filter; CVI laser, Livermore, CA), and focused on the photomultiplier tube (PMT) for detection. Unlike many commercial systems, the emmision light was not descanned, increasing the sensitivity of detection. The detector was a single photon counting R5600-P PMT (Hamamatsu, Bridgewater, NJ). The signal was preconditioned with a low noise preamplifier and a photon discriminator (Advanced Research Instrument, Boulder, CO). The digital signal was synchronized to the *x*–*y* scanner movement by custom software in order to reconstruct a two-dimensional image that was stored on the data acquisition computer. Three-dimensional reconstructions were performed offline by stacking images using the Slicer software package (Fortner Research, Sterling, VA). Vascular volume fraction calculations were performed using the NIH Image software package (NIH, Bethesda, MD). Briefly, pixel counts in each optical section were binarized, using a threshold value of ~10% of the maximum pixel value for the section, and pixels were counted to determine the fraction of pixels inside the vessel. Vascular volume fraction was then calculated assuming the thickness of the optical section to be the distance between consecutive sections.

High-Speed Intravital MPLSM

For high-speed multiphoton imaging, the multiphoton laser scanning microscope described in the previous paragraph was modified in two ways [23]. First, a rotating polygonal mirror (Lincoln Laser, Phoenix, AZ) was used to generate the line scan (along the *x* direction). The polygonal mirror has 50 facets around the perimeter and has a maximum rotation rate of 30,000 rpm. A scan line is generated at the image plane as a facet is swept across the excitation laser beam. This system has a maximum line scan rate of 25 kHz. For the slow scanning axis (along the *y* direction), a galvanometer-driven mirror (Cambridge Technology) was used. Second, due to the high signal photon flux in video-rate imaging, single photon counting detection cannot be used. Instead, the signal is acquired by a high-sensitivity PMT (R3896, Hamamatsu). A transimpedance amplifier (C1053-51, Hamamatsu) converts the current output from the PMT to an amplified voltage signal. The voltage signal is sampled with a 12-bit AD converter (AD9220EB, Analog Device, Norwood, MA) at approximately 11 MHz and is transferred to the data acquisition computer.

Animal Models

Dorsal Skin-Fold Chamber The preparation of dorsal skin-fold chambers (Figure 1) has been described previously [25]. Briefly, the back of a mouse was shaven and depilated, and two mirror-image titanium frames were mounted so as to fix the extended double layer of skin between the frames. One 15-mm-diameter layer of skin was excised leaving the striated muscle, subcutaneous tissue, and epidermis of the opposite side. The tissue was covered with a glass cover slip mounted into the frame. The surgeries were preformed in male SCID mice bred and maintained in our defined flora animal facility. Some chambers were implanted with T-241 fibrosarcoma to image tumor vasculature or BA-HAN-1C rhabdomyosarcoma to image L–E interactions. Prior to imaging, the animal was anesthetized and given either a 0.1-ml intravenous injection of 2.5% 2×10^6 MW FITC-dextran (Molecular Probes, Eugene, OR) by tail vein cannulation for vascular density measurement or a 0.05 ml intravenous injection of 0.1% rhodamine 6-G (Sigma) for L–E interaction measurement. The animal was fixed to a metal plate designed to stabilize the chamber. The FITC-dextran was excited by multiphoton absorption allowing visualization of microvasculature. Images 100–300 μm deep were obtained in both non-tumor– and tumor–bearing dorsal windows. Tumors imaged were ~1–2 mm thick.

Mouse Tail Model The experimental procedure used for microlymphangiography in the mouse tail has been described previously [26]. Briefly, an anesthetized female nude mouse was mounted on a metal plate designed for imaging the tail lymphatics on an inverted microscope. The tail was stabilized and a 5-μl injection of 2.5% 2×10^6 MW FITC-dextran (Molecular Probes) was given in the interstitial space at the tip of the tail using a 30-1/2-gauge needle (Figure 1). The FITC-dextran was taken up by lymphatics and served as a marker of functional lymphatics. Images up to 450 μm deep were obtained.

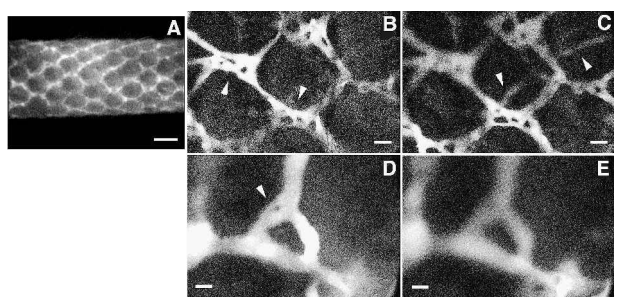

Figure 2. *Microlymphangiography in the tail of nude mice. (A) Hexagonal, superficial lymphatic pattern in the tail visualized using epifluorescence microscopy. With this technique, it appears as if the hexagonal mesh is composed of single vessels. (B) Image taken using 10× water immersion objective at a depth of 100 μm below the surface of the skin. Arrowheads point to the multiple small vessels that make up the hexagonal mesh. This fine detail is not distinguishable at the same magnification using epifluorescence. (C) Image taken using 10× water immersion objective at a depth of 225 μm below the surface of the skin. Arrowheads point to deeper draining lymphatics not visible using traditional epifluorescence microscopy. (D) Image taken using 20× water immersion objective at a depth of 100 μm below the surface of the skin. Arrowhead points to a cell (presumably a leukocyte) in the lymphatic vessel. (E) Image taken using 20× water immersion objective at a depth of 150 μm below the surface of the skin. Due to the curvature of the surface of the mouse tail, all cited depths are estimates of the average depth below the surface of the skin in the image. The scale bars represent 500 μm (A), 100 μm (B and C), and 50 μm (D and E).*

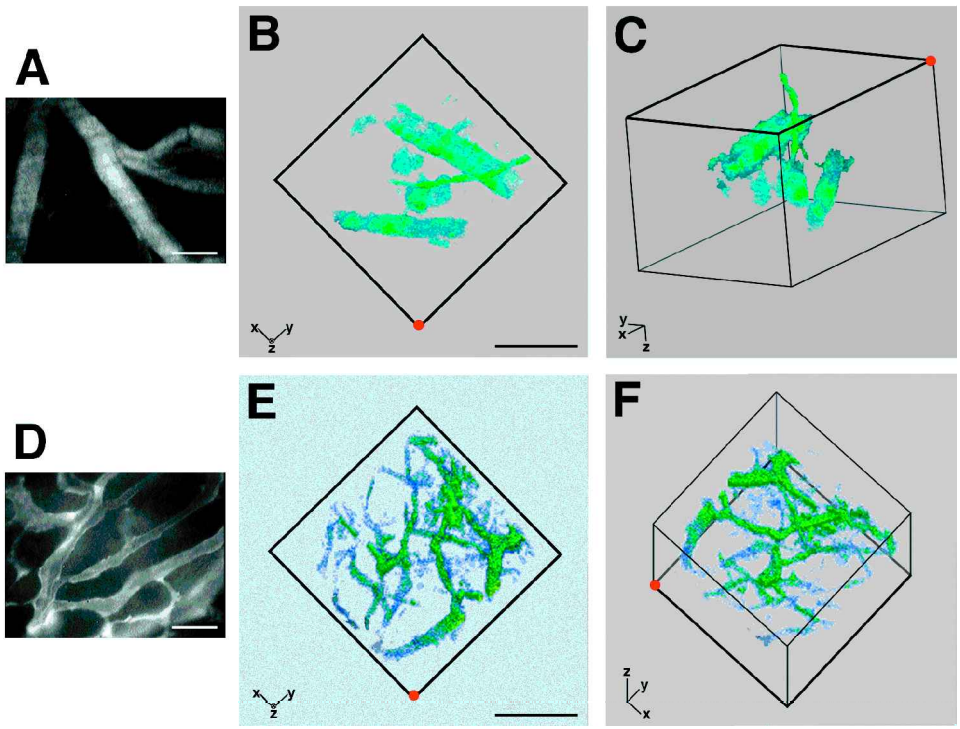

Figure 3. *Images of non-tumor (A, B, C)- and tumor-bearing (D, E, F) mouse dorsal skin obtained using the dorsal skin-fold preparation. (A) Epifluorescence image of non-tumor-bearing dorsal skin shows normal vessel density and tortuosity. (B, C) MPLSM images of non-tumor-associated mouse vasculature also show normal vessel density and tortuosity but at considerably greater depth (~200 μm). These images illustrate the three-dimensional reconstructive capability of MPLSM. The image shown in (B) represents the view looking down into the dorsal chamber from the surface of the chamber. (The z axis in the lower left points into the page.) The image in (C) is a three-dimensional representation obtained by rotating the image in (B) as indicated by the axes in the lower left. The origin of the axes is fixed to the same corner of the cube (indicated by the red dot) in both (B) and (C) and the face of the cube indicated by the darker lines in (C) is the face closest to the reader in (B). The images were obtained using a 20× objective and span a depth of ~200–300 μm. (D) Epifluorescence image of tumor grown in dorsal skin-fold chamber illustrates the increased vessel density and tortuosity characteristic of neoplastic tissue, but yields only a surface-weighted picture of the microvascular architecture. (E, F) MPLSM images of tumors grown in the dorsal skin-fold preparation illustrate the chaotic vascular network in greater detail and demonstrate that increased vessel density and tortuosity persist even at greater depths. The ability to image deeper provides a more accurate picture of the microvascular architecture and allows for more precise quantification of vessel density. As in (B) and (C), the image shown in (E) represents the view looking down into the dorsal chamber from the surface of the chamber. (Again, the z axis in the lower left points into the page.) The image in (F) is a three-dimensional representation obtained by rotating the image in (E) as indicated by the axes in the lower left. As before, the origin of the axes is fixed to the same corner of the cube (indicated by the red dot) in both (E) and (F) and the face of the cube indicated by the darker lines in (F) is the face closest to the reader in (E). The images in (E) and (F) further illustrate the utility of MPLSM for viewing spatial relationships between anatomic structures in three dimensions. The images were obtained using a 20× objective and span a depth of ~200–300 μm. All scale bars represent 100 μm. Note that the reconstructions shown require thresholding of the data collected in order to make the tissue appear transparent. As a result, some small vessels are only partially visible or absent. These renderings are intended to illustrate the three-dimensional representations that can be obtained and were not used for calculation of vascular volume fraction.*

Statistical Analysis Results are presented as means ± *s.e.m.* Two sample Student's t tests for independent samples of equal variances were performed to compare sample means. Statistical significance was based on p values smaller than 5%.

Results and Discussion

MPLSM of Lymphatics Show First High-Resolution Images of Microanatomy In Vivo

Microlymphangiography has been used to evaluate the structure and function of lymphatic vessels in the mouse tail [26–29]. Under epifluorescence, the regular hexagonal mesh pattern of the collecting lymphatics is readily apparent (Figure 2A), but much of the anatomical detail is obscured. A detailed anatomical study of collecting lymphatics has yet to be performed due to the limitations of epifluorescence microscopy. We performed microlymphangiography in the tails of nude mice with MPLSM (Figure 2B,C,D,E). The MPLSM images reveal morphological features not discernible using epifluorescence microscopy. The vertices of the hexagonal mesh along with some of the vessels on the sides are made up of small vessels merging together; these appear to be single vessels in epifluorescence images. As a result, measurements of lymphatic vessels in the tails of nude mice taken using MPLSM (mean diameter = 40.6 ± 1.4 μm; n = 141 vessels from 19 animals) were smaller ($p < .005$) than lymphatics imaged using epifluorescence microscopy (mean diameter = 54.1 ± 2.1 μm; n = 55 vessels from eight animals). In addition, the deeper, draining vessels, which have not been imaged previously, can also now be seen due to the inherent z resolution and increased depth of imaging of MPLSM (Figure 2C). Such detailed images play an important role in understanding the creation of new lymphatic vessels (lymphangiogenesis), as the

temporal dynamics of microanatomical development can now be studied in a noninvasive manner. As growth factors with putative lymphangiogenic or antilymphangiogenic activity are discovered, MPLSM will play a crucial role in investigating their effect in vivo on the growth of new lymphatics or the inhibition of this process.

The development of new tumor models, in combination with MPLSM, presents opportunities to answer some fundamental questions of tumor biology. For instance, elevated interstitial fluid pressure in solid tumors [30–34] suggests the lack of a functional lymphatic system. However, the existence of functional lymphatics in tumors is still a subject of debate due to the lack of a conclusive study. With tenfold greater depth of imaging, a definitive answer to this question may begin to emerge. As another example, the details underlying the mechanism(s) of lymphatic metastasis are not well understood. MPLSM has the resolution to image single cells in lymphatic vessels (Figure 2D), a capability that could be enhanced by the use of reporter genes such as green fluorescent protein (GFP) [35,36]. Insight into how lymphatic metastasis occurs may suggest new therapeutic targets for future treatments. As more is learned about the molecular differences between vascular and lymphatic endothelium, cell-specific markers will become available, allowing for the study of angiogenesis and lymphangiogenesis on the molecular level. Additionally, cell-specific markers will allow monitoring of treatments aimed at enhancing or inhibiting blood vessel and lymphatic growth.

High-Resolution Images Show Heterogeneous, Tortuous Tumor Vasculature

Images of blood vessels in non-tumor-bearing dorsal windows obtained using MPLSM technology (Figure 3B,C) add deeper, three-dimensional structure to the planar projections provided by epifluorescence (Figure 3A). These vessels exhibited normal density and tortuosity. In contrast, the vasculature of the T-241 fibrosarcoma was highly tortuous and had increased vascular density both at the surface (~40–50 μm) seen using epifluorescence (Figure 3D) and deeper (~200 μm) in the tumor imaged using MPLSM (Figure 3E,F). The images obtained using MPLSM were used to calculate vascular volume fraction. The ratio of vessel volume to tissue volume in tumor tissue (Figure 3E,F) was 0.199 compared to 0.098 in normal tissue (Figure 3B,C). This quantification demonstrates the potential for performing an improved angiogenic assay using MPLSM. Such an approach may prove invaluable for studying and accurately assessing the effectiveness of various antiangiogenic agents as potential cancer treatments.

High-Speed MPLSM Allows Study of Short Time Scale Phenomena

Video-rate imaging is necessary to study physiologic phenomena occurring on time scales shorter than one second. We have used high-speed MPLSM to measure the L–E interactions in normal and tumor blood vessels as deep as 350 μm in tissue (Figure 4A–H). In the BA-HAN-1C rhabdomyosarcoma (Figure 4F–H), there was no difference ($p > .05$) in leukocyte flux (16.4 ±1.8 cells/30 sec) or percentage of rolling cells (30.0 ± 3.7%)($n = 10$ vessels from two animals) when compared to normal vessels (Figure 4A–E) in the skin (16.4 ± 1.8 cells/30 sec and 20.5 ± 6.5%; $n = 6$ vessels from two animals). This suggests that the rhabdomyosarcoma does not produce cytokines that stimulate the endothelium. The absence of an increased leukocyte response deep in this tumor tissue explains, at least in part, the inability of the host immune system to clear all tumor cells. MPLSM will help to identify conditions in which L–E

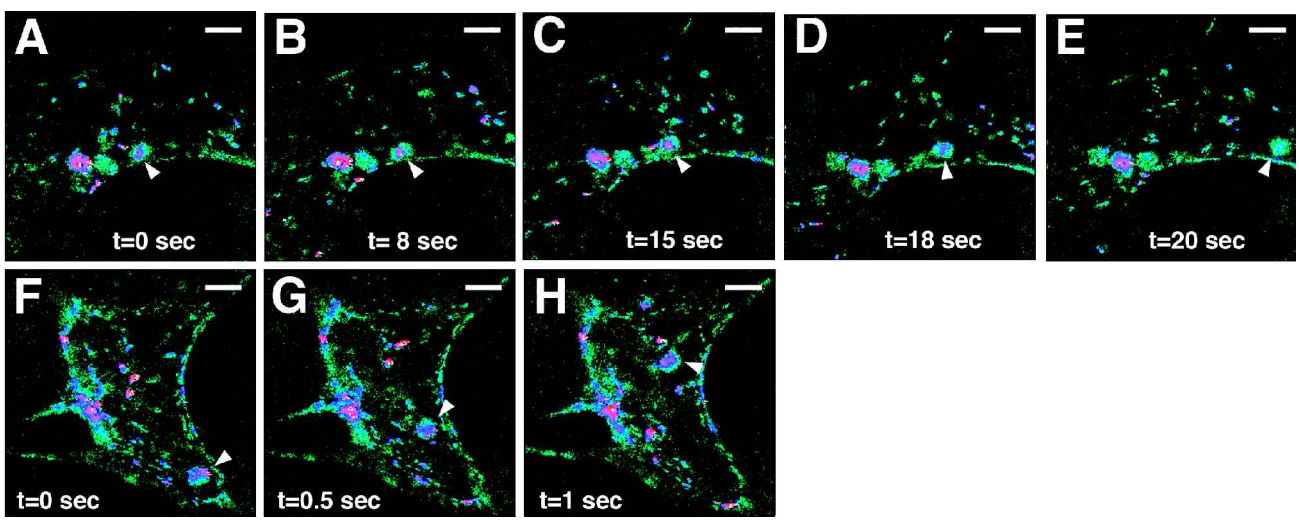

Figure 4. *Single frames extracted from movies acquired using high-speed MPLSM of L–E interaction in the dorsal skinfold chamber. (A–E) Vessel in a non-tumor-bearing chamber imaged at a depth of 150 μm below chamber window. The elapsed times are shown. The arrowhead follows a single leukocyte that had adhered to the vessel wall (A, B), released (C), and rolled along the vessel wall (D, E). Leukocytes and platelets can be seen in the blood flow which has an average velocity of 80 μm/sec. (F–H) Vessel in BA-HAN-1C rhabdomyosarcoma growing in a dorsal skinfold chamber imaged at a depth of 200 μm below the chamber window. The elapsed times are shown. The arrowhead follows a single leukocyte traveling with the blood flow, not interacting with the vessel wall. The blood flow has an average velocity of 220 μm/sec. All scale bars represent 40 μm.*

interactions are increased, which, in turn, could lead to novel immunotherapies for cancer.

With the development of in vivo fluorescent reporters such as GFP [2,4,7,35–38], high-speed MPLSM will permit the direct observation of various steps in metastasis. Tumor cell extravasation at the primary site, circulation, and intravasation at the metastatic site are not understood and very difficult to observe directly due to the inability to image at depth with high resolution. High-speed MPLSM will be able to capture these phenomena. As new molecular markers are developed, the power of high-speed MPLSM can be used to monitor many phases of cell response to treatment, including cell proliferation and apoptosis. In addition, although steady blood velocity has been measured with MPLSM [19,21], unsteady, heterogeneous, and/or reversing flow, common phenomena in tumors [39], can also be analyzed with high-speed MPLSM.

Conclusion

We have demonstrated the utility of MPLSM to study biological events in vivo and, for the first time, described the use of high-speed MPLSM in vivo. The inherent three-dimensional resolution deep in tissue and low phototoxicity make MPLSM ideal for these applications. The ability to image at video-rate further increases the utility of this technique, expanding the range of problems that can be addressed to include phenomena that occur on short time scales. We have illustrated the use of MPLSM and high-speed MPLSM to address questions relevant to tumor biology; high-resolution imaging of functional lymphatics, tumor blood vessels, and the interaction of leukocytes with tumor endothelium. Future studies based on these techniques may finally resolve long-standing, unanswered questions about the molecular, cellular, and integrative biology of solid tumors. MPLSM will allow the deeper, often poorly vascularized and treatment-resistant parts of the tumor to be studied, which cannot be done with epifluorescence microscopy. The continued application and development of in vivo MPLSM techniques for measuring biological parameters (e.g., pO_2, pH, ligand–receptor interactions, promoter activity), combined with fluorescent molecular markers, can determine the regulation and function of genes (see cover) and give novel insight into the recently sequenced genome.

Acknowledgments

The authors thank Y. Chen, C. Dong, K. King, D. Fukumura, T. Gohongi, A. Kadambi, and J. Kahn for their technical expertise. They also thank E. Brown, K. Burton, E. di Tomaso, and L. Munn for their insightful criticism of the manuscript. This work was supported by an NCI Outstanding Investigator Grant (R35-CA 56591), a Bioengineering Research Partnership Grant (R24 CA85140), and National Foundation for Cancer Research Project Grant to RKJ, and grants ACS RPG9805801CCE and NIH R29GM56486-01 to PTCS. TPP is a recipient of the Whitaker Health Sciences Fund Fellowship.

References

[1] Jain RK, Munn LL, Fukumura D (2001). Transparent window models and intravital microscopy. In: *Tumor models in cancer research*. BA Teicher, Ed. Humana Press, Totowa, NJ.

[2] Fukumura D, Xavier R, Sugiura T, Chen Y, Park EC, Lu N, Selig, M, Nielsen G, Taksir T, Jain RK, Seed B (1998). Tumor induction of VEGF promoter activity in stromal cells. *Cell.* **94**:715-725.

[3] Dellian, M, Yuan, F, Trubetskoy VS, Torchilin VP, Jain RK (2000). Vascular permeability in a human tumour xenograft: Molecular charge dependence. *Br J Cancer.* **82**:1513-1518.

[4] Pfeifer A, Kessler T, Yang M, Baranov E, Kootstra N, Cheresh DA, Hoffman RM, Verma, IM (2001). Transduction of liver cells by lentiviral vectors: Analysis in living animals by fluorescence imaging. *Mol Ther: J Am Soc Gene Ther.* **3**:319-322.

[5] Kadambi A, Carreira CM, Yun CO, Padera TP, Dolmans DE, Carmeliet P, Fukumura D, Jain RK (2001). Vascular endothelial growth factor (VEGF)-C differentially affects tumor vascular function and leukocyte recruitment: Role of VEGF-receptor 2 and host VEGF-A. *Cancer Res.* **61**:2404-2408.

[6] Jain RK, Munn LL, Fukumura D, Melder RJ (1999). In vitro and in vivo quantification of adhesion between leukocytes and vascular endothelium. *Methods Mol Med.* **18**:553-575.

[7] Hoffman RM (2001). Visualization of GFP-expressing tumors and metastasis in vivo. *Biotechniques.* **30**:1016-1026.

[8] Pluen A, Boucher Y, Ramanujan S, McKee TD, Gohongi T, di Tomaso E, Brown EB, Izumi Y, Campbell RB, Berk DA, Jain RK (2001). Role of tumor–host interactions in interstitial diffusion of macromolecules: Cranial vs. subcutaneous tumors. *Proc Natl Acad Sci USA.* **98**:4628-4633.

[9] Chary SR, Jain RK (1989). Direct measurement of interstitial convection and diffusion of albumin in normal and neoplastic tissues by fluorescence photobleaching. *Proc Natl Acad Sci USA.* **86**:5385-5389.

[10] Berk DA, Yuan F, Leunig M, Jain RK (1997). Direct in vivo measurement of targeted binding in a human tumor xenograft. *Proc Natl Acad Sci USA.* **94**:1785-1790.

[11] Helmlinger G, Yuan F, Dellian M, Jain RK (1997). Interstitial pH and pO2 gradients in solid tumors in vivo: High-resolution measurements reveal a lack of correlation. *Nat Med.* **3**:177-182.

[12] Jain RK (1998). The next frontier of molecular medicine: Delivery of therapeutics. *Nat Med.* **4**:655-657.

[13] Jain RK (1999). Understanding barriers to drug delivery: High resolution in vivo imaging is key. *Clin Cancer Res.* **5**:1605-1606.

[14] Squirrell JM, Wokosin DL, White JG, Bavister BD (1999). Long-term two-photon fluorescence imaging of mammalian embryos without compromising viability. *Nat Biotechnol.* **17**:763-767.

[15] Denk W, Strickler JH, Webb, WW (1990). Two-photon laser scanning fluorescence microscopy. *Science.* **248**:73-76.

[16] Yuste R, Denk W (1995). Dendritic spines as basic functional units of neuronal integration. *Nature.* **375**:682-684.

[17] Masters BR, So PTC, Gratton E (1997). Multiphoton excitation fluorescence microscopy and spectroscopy of in vivo human skin. *Biophys J.* **72**:2405-2412.

[18] Svoboda K, Denk W, Kleinfeld D, Tank DW (1997). In vivo dendritic calcium dynamics in neocortical pyramidal neurons. *Nature.* **385**:161-165.

[19] Kleinfeld D, Mitra PP, Helmchen F, Denk W (1998). Fluctuations and stimulus-induced changes in blood flow observed in individual capillaries in layers 2 through 4 of rat neocortex. *Proc Natl Acad Sci USA.* **95**:15741-15746.

[20] Lendvai B, Stern EA, Chen B, Svoboda K (2000). Experience-dependent plasticity of dendritic spines in the developing rat barrel cortex in vivo. *Nature.* **404**:876-881.

[21] Brown EB, Campbell RB, Tsuzuki Y, Xu L, Carmeliet P, Fukumura D, Jain RK (2001). In vivo measurement of gene expression, angiogenesis and physiological function in tumors using multiphoton laser scanning microscopy. *Nat Med.* **7**:864-868.

[22] Göppert-Mayer M (1931). Über Elementarakte mit zwei Quantensprüngen. *Ann Phys (Leipzig).* **9**:273-294.

[23] Kim KH, Buehler C, So PTC (1999). High-speed, two-photon scanning microscope. *Appl Opt.* **38**:6004-6009.

[24] So PTC, French T, Yu WM, Berland KM, Dong CY, Gratton E (1996). Two-Photon fluorescence microscopy; time-resolved and intensity imaging. In: *Fluorescence imaging and microscopy*. XF Wang, B Herman, Eds. Wiley, New York.

[25] Leunig M, Yuan F, Menger MD, Boucher Y, Goetz AE, Messmer K, Jain RK (1992). Angiogenesis, microvascular architecture, microhemodynamics, and interstitial fluid pressure during early growth of human adenocarcinoma LS174T in SCID mice. *Cancer Res.* **52**:6553-6560.

[26] Leu AJ, Berk DA, Yuan F, Jain RK (1994). Flow velocity in the superficial lymphatic network of the mouse tail. *Am J Physiol.* **267**:H1507-H1513.

[27] Berk DA, Swartz MA, Leu AJ, Jain RK (1996). Transport in lymphatic capillaries: II. Microscopic velocity measurement with fluorescence photobleaching. *Am J Physiol.* **270**:H330-H337.

[28] Swartz MA, Berk DA, Jain RK (1996). Transport in lymphatic capillaries: I. Macroscopic measurements using residence time distribution theory. *Am J Physiol.* **270**:H324-H329.

[29] Leu AJ, Berk DA, Lymboussaki A, Alitalo K, Jain RK (2000). Absence of functional lymphatics within a murine sarcoma: A molecular and functional evaluation. *Cancer Res.* **60**:4324-4327.

[30] Boucher Y, Kirkwood JM, Opacic D, Desantis M, Jain RK (1991). Interstitial hypertension in superficial metastatic melanomas in humans. *Cancer Res.* **51**:6691-6694.

[31] Roh HD, Boucher Y, Kalnicki S, Buchsbaum R, Bloomer WD, Jain RK (1991). Interstitial hypertension in carcinoma of uterine cervix in patients: Possible correlation with tumor oxygenation and radiation response. *Cancer Res.* **51**:6695-6698.

[32] Less JR, Posner MC, Boucher Y, Borochovitz D, Wolmark N, Jain RK (1992). Interstitial hypertension in human breast and colorectal tumors. *Cancer Res.* **52**:6371-6374.

[33] Gutmann R, Leunig M, Feyh J, Goetz AE, Messmer K, Kastenbauer E, Jain RK (1992). Interstitial hypertension in head and neck tumors in patients: Correlation with tumor size. *Cancer Res.* **52**:1993-1995.

[34] Boucher Y, Salehi H, Witwer B, Harsh GR, Jain RK (1997). Interstitial fluid pressure in intracranial tumours in patients and in rodents. *Br J Cancer.* **75**:829-836.

[35] Tsien RY (1998). The green fluorescent protein. *Annu Rev Biochem.* **67**:509-544.

[36] Lippincott-Schwartz J, Snapp E, Kenworthy A (2001). Studying protein dynamics in living cells. *Nat Rev Mol Cell Biol.* **2**:444-456.

[37] Naumov GN, Wilson SM, MacDonald IC, Schmidt EE, Morris VL, Groom AC, Hoffman RM, Chambers AF (1999). Cellular expression of green fluorescent protein, coupled with high-resolution in vivo videomicroscopy, to monitor steps in tumor metastasis. *J Cell Sci.* **112**:1835-1842.

[38] Yang M, Baranov E, Li XM, Wang JW, Jiang P, Li L, Moossa AR, Penman S, Hoffman RM (2001). Whole-body and intravital optical imaging of angiogenesis in orthotopically implanted tumors. *Proc Natl Acad Sci USA.* **98**:2616-2621.

[39] Jain RK (1997). The Eugene M. Landis Award Lecture 1996. Delivery of molecular and cellular medicine to solid tumors. *Microcirculation.* **4**:1-23.